Characterisation of the phase-transformation behaviour of $Ce_2O(CO_3)_2 \cdot H_2O$ clusters synthesised from $Ce(NO_3)_3 \cdot 6H_2O$ and urea

Anita M. D'Angelo,[1] Nathan A. S. Webster,[2] and Alan L. Chaffee[1,a)]
[1] *CRC for Greenhouse Gas Technologies (CO2CRC), School of Chemistry, Monash University, Clayton, VIC 3800 Australia*
[2] *CSIRO Mineral Resources Flagship, Private Bag 10, Clayton South, VIC 3169, Australia*

(Received 3 September 2014; accepted 30 September 2014)

X-ray diffraction (XRD) was used to determine the temperature at which the transformation of $Ce_2O(CO_3)_2 \cdot H_2O$ to ceria (CeO_2) occurs under both a flow of nitrogen and air as a function of temperature. The $Ce_2O(CO_3)_2 \cdot H_2O$ synthesised from $Ce(NO_3)_3 \cdot 6H_2O$ and urea was further investigated using thermal gravimetric analysis (TGA), scanning electron microscopy (SEM), and transmission electron microscopy (TEM). XRD results indicate that, under a flow of nitrogen, CeO_2 is formed at temperatures greater than 500 °C and that this occurs via an as yet unidentified intermediate phase, which is present between 430 and 540 °C. Results obtained by the XRD correspond to those obtained using TGA, which show weight losses commencing at 430 and at 465 °C. No further weight loss occurs above 540 °C, because of the formation of CeO_2 as the stable product. The crystallite size was also determined and observed to increase with increasing temperature. Under a flow of air the transformation occurred at a lower temperature, as CeO_2 was formed at 250 °C. SEM and TEM reveal the particles have a rod-shaped morphology which is retained after calcination. These results may be used to optimise synthesis methods to minimise crystallite size growth and reduce sintering that is undesirable in many applications, particularly catalysis. © *2014 International Centre for Diffraction Data.*
[doi:10.1017/S0885715614001080]

Key words: cerium oxide, nanorods, variable-temperature XRD, intermediate

I. INTRODUCTION

Ceria (CeO_2) is commonly exploited for its oxygen-storage capacity (OSC) and oxygen-buffering capacity in solid-oxide fuel cells (SOFCs; da Costa *et al.*, 2012; Kearney *et al.*, 2012), and automotive three-way catalysis (Kašpar *et al.*, 1999). For solid-oxide fuel cell applications, CeO_2-based anodes have been considered as potential materials owing to their high oxygen mobility, which is necessary for hydrogen oxidation. Similarly, as a three-way catalyst, CeO_2 is required to simultaneously reduce NO_x and oxidise CO and hydrocarbons; this is achieved through its ability to uptake and release oxygen reversibly. Oxygen pulses are buffered under rich (reducing) or lean (oxidising) conditions as a result of ceria's redox ability (i.e. OSC) such that a corresponding change in Ce^{4+}/Ce^{3+} valence state occurs.

Catalysts with a high OSC are desirable as this can result in higher catalytic activity and higher stability. In a series of aluminium-doped CeO_2–zirconia (ZrO_2) supported palladium–alumina catalysts, the high OSC (583 μmol O g^{-1}) of $Ce_{0.5}Zr_{0.3}Al_{0.2}O_{1.9}/Pd/\gamma\text{-}Al_2O_3$ was found to correspond with the highest CO oxidation activity and good stability (Dong *et al.*, 2013). Similarly, the higher OSC of Tb-doped CeO_2–ZrO_2 catalysts developed for the steam reforming of propane were also shown to be more durable as carbon formation was minimised because of a greater number of oxygen species able to react and form CO_2 at a lower temperature (Harshini *et al.*, 2013).

The ability of CeO_2 to act as an effective catalyst is strongly dependent on the synthesis method employed which, in turn, affects factors such as crystallite size and morphology. CeO_2 exhibiting enhanced catalytic activity and higher extent of reduction have been associated with nano-sized rather than micron-sized particles (Soykal *et al.*, 2012). The higher catalytic ability of nanoparticles is generally attributed to a greater amount of Ce^{3+} and the associated oxygen vacancies required to balance charge (Hua *et al.*, 2012). An increase in Ce^{3+} was observed when comparing nanoparticles to micron sized particles; however, for particles below 10 nm the concentration of Ce^{3+} was found to be independent of particle size or the synthesis precursor (Revoy *et al.*, 2013). In addition, Paun *et al.* (2012) determined that for 2–10 nm-sized polyhedrals the concentration of Ce^{3+} did not change with particle size.

The aforementioned oxygen vacancies can act as potential adsorption sites and have been associated with OSC more so than other properties, such as surface area. Mamontov *et al.* (2000) showed CeO_2 defect concentrations declined above 760 °C, corresponding to a decrease in OSC from 217 to 62 μmol O_2 g^{-1} at 750 and 800 °C, respectively. At higher temperatures these species are destroyed and consequently result in the reduction of the OSC (Deraz and Alarifi, 2009). Ensuring crystallite growth is minimised may assist in the preservation of vacancies and result in the OSC being maintained.

The morphology of the particles can also alter the extent of defects as nanorods have been found to possess a greater

---

a) Author to whom correspondence should be addressed. Electronic mail: Alan.Chaffee@monash.edu

amount of stable Ce^{3+}, defects, and surface active sites, than nanocubes and nano-octahedra (Wu *et al.*, 2010). The number of these crystal-defect sites is determined by surface terminations where, for the low-index planes, the highest vacancy formation energy follows the trend (111) > (100) > (110) (Nolan *et al.*, 2005b). The presence of vacancies was found by Nolan *et al.* (2005a) not to be linked to the surface stability as the most stable CeO_2 surface was (111) followed by (110) and then (100). The more reactive (100) sites disappear when the particle size increases above 10 nm (Wang and Feng, 2003). The dominant exposed planes for nanocubes and nano-octahedra were (100) and (111), respectively (Florea *et al.*, 2013) and the most prominent exposed surface for nanorods are the (100) and (110) planes, which may explain their higher reactivity in CO oxidation (Zhou *et al.*, 2005). Nanorods have also been found to have a higher OSC (554 μmol O g^{-1}) in comparison with nanopolyhedra (318 μmol O g^{-1}) and nanocubes (353 μmol O g^{-1}) (Mai *et al.*, 2005). Other applications where nanorods have exhibited higher reactivity than nanocubes or nano-octahedra include as a support for vanadia catalysts for the oxidative dehydrogenation of isobutane (Wu *et al.*, 2012) and as a support for gold in CO oxidation, butadiene hydrogenation, and benzylic alcohol oxidation (Guan *et al.*, 2011).

In this work, we investigated the oxidation of $Ce_2O(CO_3)_2{\cdot}H_2O$ using variable-temperature X-ray diffraction (XRD) under both a flow of nitrogen and air. High catalytic activity and stability are attributed to the presence of a high number of stable Ce^{3+} vacancies, which are more abundant in nano-sized crystallites and particles with rod morphology. As the generation and preservation of these active sites is largely dependent on the synthesis method employed, understanding the oxidation pathway of the precursor may assist in maximising these species, allowing for catalyst improvement.

II. EXPERIMENTAL

A. Preparation

Cerium oxide was prepared by dissolving $Ce(NO_3)_3{\cdot}6H_2O$ (Aldrich, 99%) and an excess (15 × the total ion concentration) of urea, $CO(NH_2)_2$ (Sigma-Aldrich, 99–100.5%), in deionised water to obtain a 0.1 mol l^{-1} solution. With vigorous stirring, the solution was heated to 90 °C for 8 h. The resultant precipitate was filtered, and washed with water and ethanol (absolute, Merck) before drying in an oven at 90 °C overnight. Calcination involved heating from ambient to 700 °C at a rate of 2 °C min^{-1}, followed by isothermal treatment at 700 °C for 2 h.

Variable-temperature XRD data were collected on the precipitated material using an Inel Equinox 3000 fitted with a CPS120 position sensitive detector and a Mo tube operated at 40 kV and 40 mA. Mo*Kα* was used to significantly reduce the effects of absorption, compared with lower-energy Co or Cu*Kα*. Samples were packed into a 0.7 mm quartz capillary and stoppered with glass wool before heating to 750 °C at 5 °C min^{-1}. Data sets were collected at 1 min intervals. To determine the diffractometer zero and instrumental effects on peak width and shape, data were collected for LaB_6 (NIST 660b standard reference material). The diffraction domain length (L_{vol}) was determined using whole-pattern fitting implemented in TOPAS (Bruker AXS, 2009).

Thermal gravimetric characterisation of the precipitated material was carried out using a Mettler Toledo TGA/DSC 1. Approximately 15 mg of sample was weighed into an alumina crucible (150 μl) and heated to 800 °C in a flow of nitrogen (35 ml min^{-1}). Scanning electron microscopy (SEM) characterisation of calcined CeO_2 particle morphology and size was obtained using a FEI Nova Nano 450 FEG SEM. Samples were prepared by dispersing the powder on an aluminium stub using conductive carbon tape and coating with platinum. Transmission electron microscopy (TEM) characterisation was carried out on an FEI Tecnai G2 T20 Twin TEM fitted with a LaB_6 thermal emitter operated at 200 kV. Samples were prepared by dispersing in *n*-butyl alcohol (ChemSupply, >99%) and ultra-sonicating before dipping a carbon film (400 mesh Cu) into the solution.

III. RESULTS AND DISCUSSION

A. Phase evolution

The combination of Ce^{3+} and urea resulted in the generation of $Ce_2O(CO_3)_2{\cdot}H_2O$ (PDF No. 00-043-0602, ICDD 2010) and is consistent with the literature (Chen and Chen, 1993; Hirano and Kato, 1999b). The precipitation of $Ce_2O(CO_3)_2{\cdot}H_2O$ is reported to occur at low pH as Ce^{3+} is weakly hydrated, allowing for reaction with CO_3^{2-} (Hirano and Kato, 1999a). Upon increasing the temperature under a nitrogen atmosphere [Figure 1(a)] this phase begins to decompose at ~430 °C and persists until ~500 °C. Between 430 and 540 °C an intermediate phase is formed which has unknown crystal structure and future work will aim to determine its structural details. Reflections corresponding to the cubic fluorite structure (space group $Fm\bar{3}m$) of CeO_2 are evident at temperatures greater than 500 °C and at temperatures greater than 540 °C all reflections correspond to those of CeO_2 (PDF No. 00-034-0394, ICDD 2010). At 750 °C the lattice parameter was determined as $a = 5.445(1)$ Å.

Figure 1(b) shows the change in crystal structure of $Ce_2O(CO_3)_2{\cdot}H_2O$ with increasing temperature in air. The formation of CeO_2 occurs at approximately 250 °C with reflections corresponding to the cubic fluorite structure. This corresponds well with the oxidation temperature of 245 °C, when heated at 5 °C min^{-1} in air, as obtained by Oikawa and Fujihara (2005). There is no evidence of the formation of an intermediate as observed when the experiment was carried out under a flow of nitrogen. With increasing temperature the widths of individual reflections decrease because of an increase in crystallinity. At 750 °C the lattice parameter in air was $a = 5.421(1)$ Å. As expected, oxidation of $Ce_2O(CO_3)_2{\cdot}H_2O$ occurred at a lower temperature in air in comparison to nitrogen. In Figure 1(b), there is also the presence of an intense low-angle feature, which is first observed when $Ce_2O(CO_3)_2{\cdot}H_2O$ begins to decompose at ~225 °C and CeO_2 begins to form, and persists until ~700 °C. A similar, yet much weaker, low-angle feature was also observed in Figure 1(a) for the experiment conducted under nitrogen. These low-angle features are attributed to small-angle scattering, and future *in situ* work on a dedicated small-angle scattering instrument may allow for determination of nanoparticle size and shape evolution. This, however, is beyond the scope of the present study.

Here, an estimate of CeO_2 crystallite size was obtained by calculating L_{vol}, the diffraction domain length, and Figure 2

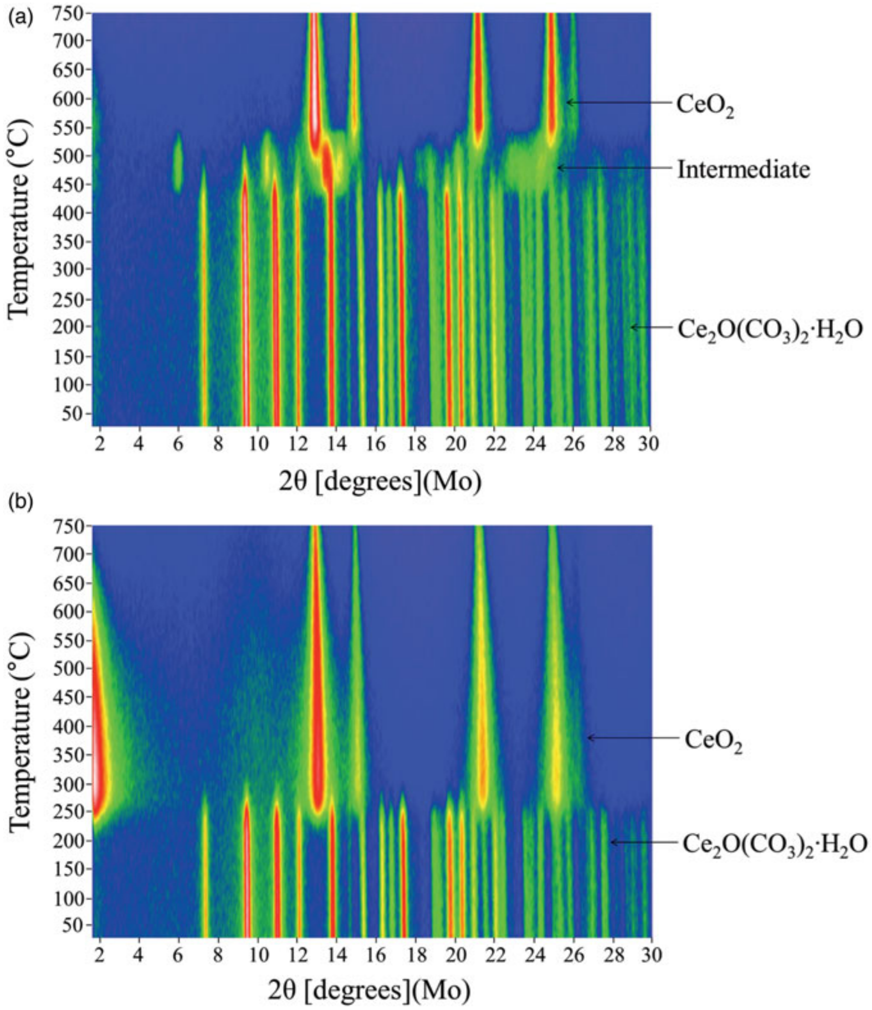

Figure 1. (Color online) Accumulated XRD data collected during heating, at 5 °C min, under (a) nitrogen and (b) air.

shows the evolution of L_{vol} as a function of temperature. When heated under nitrogen, values were calculated at temperatures greater than 550 °C only, since at this temperature $Ce_2O(CO_3)_2·H_2O$ and the intermediate phase had fully decomposed to form CeO_2 [Figure 1(a)]. As expected, L_{vol} increases with increasing temperature. In addition, the rate of increase becomes slightly greater above 700 °C. In air, L_{vol} values were calculated at temperatures greater than 260 °C only, with the rate of increase greater above ~600 °C.

The implications of generating larger crystallites from higher calcination temperatures may result in a higher CeO_2 reduction temperature. For example, the catalytic activity of CeO_2 nanorods and nanoparticles, calcined at both 700 and 900 °C, were evaluated for methane combustion, a proposed fuel for SOFCs, by Sun *et al.* (2012). A lower half methane

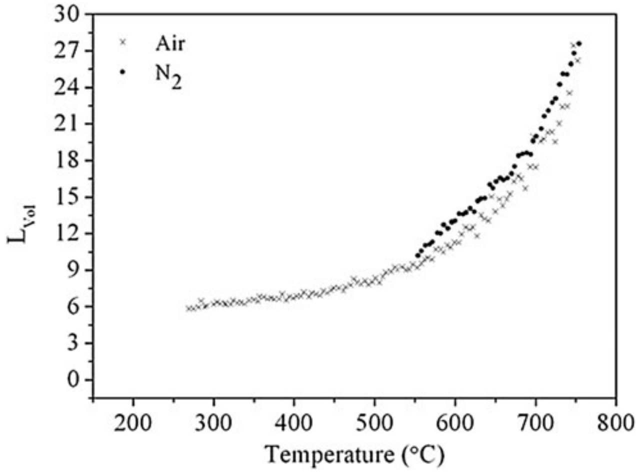

Figure 2. Evolution of the diffraction domain length, L_{vol}, of CeO_2 as a function of temperature under both nitrogen (•) and air (×) atmospheres.

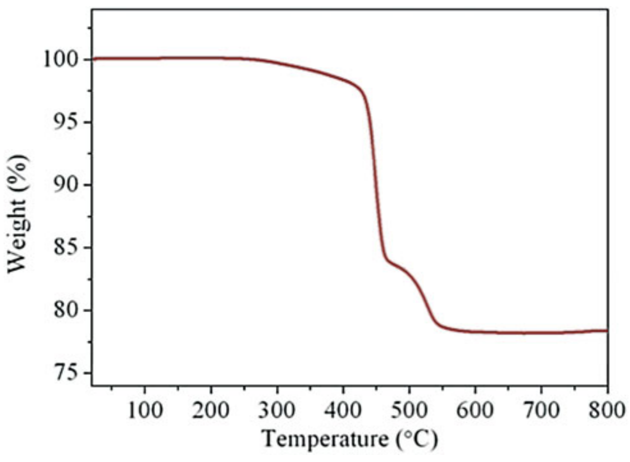

Figure 3. (Color online) TG curve of $Ce_2O(CO_3)_2·H_2O$ heated to 800 °C in nitrogen.

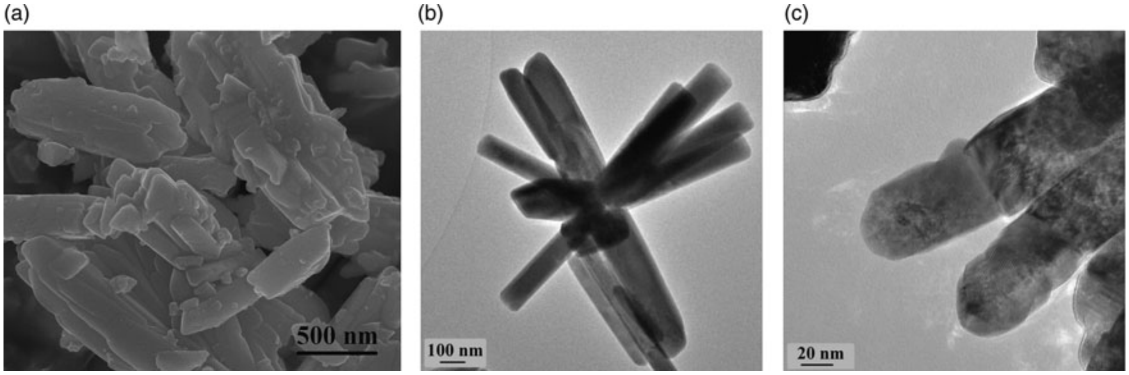

Figure 4. (a) SEM image of $Ce_2O(CO_3)_2{\cdot}H_2O$, (b) TEM image of $Ce_2O(CO_3)_2{\cdot}H_2O$, and (c) TEM image of CeO_2 generated through calcination in air from $Ce_2O(CO_3)_2{\cdot}H_2O$.

conversion-temperature (T_{50}) was obtained for both the nanorods and nanoparticles calcined at 700 °C (541 and 590 °C, respectively) rather than 900 °C (nanorods at 574 °C and nanoparticles at 645 °C). As the extent of reduction corresponds with the ability of the material to uptake oxygen, the OSC may be inhibited for larger crystallites produced from higher calcination temperatures. It has also been reported elsewhere that crystallite size is dependent on the precursor materials employed (Liu *et al.* 2013), and our future work involves investigating CeO_2 nanoparticles synthesised by other procedures and from other precursors such as Ce^{4+}/urea, Ce^{4+}/NH_4OH, and Ce^{3+}/NH_4OH.

B. Thermal gravimetric analysis (TGA)

The TG profile of $Ce_2O(CO_3)_2{\cdot}H_2O$ is shown in Figure 3 and an initial weight loss of 16% is observed at 430 °C with a second of 5.9% at 465 °C. No additional weight loss occurs after 540 °C, since the CeO_2 is fully oxidised. The temperature at which weight losses occur correspond well with the structural changes observed in Figure 1(a). The first weight loss may be attributed to the decomposition of the $Ce_2O(CO_3)_2{\cdot}H_2O$ and the second to the oxidation of the intermediate to CeO_2. There is a discrepancy between the total observed weight loss (21.9%) and theoretical weight loss (20.7%), indicating the possibility of remaining carbon and the oxide in a non-stoichiometric state ($CeO_{1.84}$). Complete oxidation to CeO_2 may be inhibited as this experiment was carried out in a low-oxygen atmosphere. In an air atmosphere, a lower amount of Ce^{3+} (ionic radius = 1.14 Å; Shannon, 1976) is expected as these are readily oxidised to Ce^{4+} (0.97 Å). This is supported by the larger lattice parameter obtained at 750 °C under nitrogen ($a = 5.445(1)$ Å), in comparison with air ($a = 5.421(1)$ Å), and likely attributed to the presence of a higher proportion of larger Ce^{3+} cations.

C. Electron microscopy

The SEM image of $Ce_2O(CO_3)_2{\cdot}H_2O$ in Figure 4(a) shows that the particles have a rod-shaped morphology with individual rods aggregated together. In Figure 4(b), the individual rods appear to grow from one shared nucleus and are approximately 100 nm in width and 500 nm in length. Following air calcination, the morphology is maintained with the individual rods comprised smaller cubic-shaped crystallites joined together by overlying facets [Figure 4(c)].

IV. CONCLUSION

CeO_2-based catalysts exhibiting higher catalytic activity and stability have been associated with a high OSC and attributed to the presence of a high number of stable Ce^{3+} and vacancies. Nano-sized rather than micron-sized particles, and those with rod-shape morphology, generally possess a greater amount of these defects and surface-active sites. As the synthesis method is a major factor in the properties of the resulting catalyst, the transformation behaviour of $Ce_2O(CO_3)_2{\cdot}H_2O$ rod clusters synthesised from $Ce(NO_3)_3{\cdot}6H_2O$ and urea was characterised using the XRD under a flow of both nitrogen and air. In a nitrogen atmosphere, the transformation occurs through an intermediate present between 430 and 540 °C with an unknown crystal structure and, above 500 °C, CeO_2 began to form. In air, the transformation occurred at a lower temperature (250 °C). TGA data correspond with those results obtained using XRD and show a weight loss at 430 °C with a second at 465 °C. As expected, the crystallite size also increased with increasing temperature. These results may be used to optimise the synthesis methods of cerium-based catalysts.

ACKNOWLEDGEMENTS

We acknowledge the financial support provided by the Australian Government through its Cooperative Research Centre programme and through the Australian National Low Emissions Coal Research Development (ANLEC R&D) scheme. ANLEC R&D is supported by Australian Coal Association Low Emission Technology Limited and the Australian Government through the Clean Energy Initiative.

Bruker AXS. (**2009**). TOPAS V4.2 (computer software), Bruker AXS Inc., Madison, USA.

Chen, P. L. and Chen, I. W. (**1993**). “Reactive cerium (IV) oxide powders by the homogeneous precipitation method,” J. Am. Ceram. Soc. **76**, 1577–1583.

da Costa, L. O., da Silva, A. M., Noronha, F. B., and Mattos, L. V. (**2012**). “The study of the performance of Ni supported on gadolinium doped ceria SOFC anode on the steam reforming of ethanol,” Int. J. Hydrogen Energy **37**, 5930–5939.

Deraz, N. M. and Alarifi, A. (**2009**). “Structural, surface and catalytic properties of nano-sized ceria catalysts,” Adsorpt. Sci. Technol. **27**, 413–422.

Dong, Q., Yin, S., Guo, C., Wu, X., Kimura, T., and Sato, T. (**2013**). “Aluminium doped ceria–zirconia supported palladium-alumina catalyst with high oxygen storage capacity and CO oxidation activity," Mater. Res. Bull. **48**, 4989–4992.

Florea, I., Feral-Martin, C., Majimel, J., Ihiawakrim, D., Hirlimann, C., and Ersen, O. (**2013**). "Three-dimentional tomographic analyses of CeO_2 nanoparticles," Cryst. Growth Des. **13**, 1110–1121.

Guan, Y., Ligthart, D. A. J. M., Pirgon-Galin, Ö., Pieterse, J. Z., Santen, R., and Hensen, E. M. (**2011**). "Gold stabilized by nanostructured ceria supports: nature of the active sites and catalytic performance," Top. Catal. **54**, 424–438.

Harshini, D., Kim, Y., Nam, S. W., Lim, T. H., Hong, S. A., and Yoon, C. W. (**2013**). "Influence of terbium doping on oxygen storage capacity of ceria–zirconia supports: enhanced durability of Ni catalysts for propane steam reforming," Catal. Lett. **143**, 49–57.

Hirano, M., and Kato, E. (**1999a**). "Hydrothermal synthesis of nanocrystalline cerium(IV) oxide powders," J. Am. Ceram. Soc. **82**, 786–788.

Hirano, M., and Kato, E. (**1999b**). "Hydrothermal synthesis of two types of cerium carbonate particles," J. Mater. Sci. Lett. **18**, 403–405.

Hua, G., Zhang, L., Fei, G., and Fang, M. (**2012**). "Enhanced catalytic activity induced by defects in mesoporous ceria nanotubes," J. Mater. Chem. **22**, 6851–6855.

ICDD (**2010**). PDF-2 2010 (Database), edited by Soorya Kabekkodu (International Centre for Diffraction Data, Newtown Square, PA, USA).

Kašpar, J., Fornasiero, P., and Graziani, M. (**1999**). "Use of CeO_2-based oxides in the three-way catalysis," Catal. Today **50**, 285–298.

Kearney, J., Hernández-Reta, J. C., and Baker, R. T. (**2012**). "Redox and catalytic properties of Ce–Zr mixed oxide nanopowders for fuel cell applications," Catal. Today **180**, 139–147.

Liu, Z., Ding, D., Liu, M., Li, X., Sun, W., Xia, C., and Liu, M. (**2013**). "Highly active $Sm_{0.2}Ce_{0.8}O_{1.9}$ powders of very low apparent density derived from mixed cerium sources," J. Power Sources **229**, 277–284.

Mai, H. X., Sun, L. D., Zhang, Y. W., Si, R., Feng, W., Zhang, H. P., Liu, H. C., and Yan, C. H. (**2005**). "Shape-selective synthesis and oxygen storage behavior of ceria nanopolyhedra, nanorods, and nanocubes," J. Phys. Chem. B **109**, 24380–24385.

Mamontov, E., Egami, T., Brezny, R., Koranne, M., and Tyagi, S. (**2000**). "Lattice defects and oxygen storage capacity of nanocrystalline ceria and ceria–zirconia," J. Phys. Chem. B **104**, 11110–11116.

Nolan, M., Grigoleit, S., Sayle, D. C., Parker, S. C., and Watson, G. W. (**2005a**). "Density functional theory studies of the structure and electronic structure of pure and defective low index surfaces of ceria," Surf. Sci. **576**, 217–229.

Nolan, M., Parker, S. C., and Watson, G. W. (**2005b**). "The electronic structure of oxygen vacancy defects at the low index surfaces of ceria," Surface Sci. **595**, 223–232.

Oikawa, M., and Fujihara, S. (**2005**). "Crystal growth of $Ce_2O(CO_3)_2{\cdot}H_2O$ in aqueous solutions: film formation and samarium doping," J. Solid State Chem. **178**, 2036–2041.

Paun, C., Safonova, O. V., Szlachetko, J., Abdala, P. M., Nachtegaal, M., Sa, J., Kleymenov, E., Cervellino, A., Krumeich, F., and van Bokhoven, J. A. (**2012**). "Polyhedral CeO_2 nanoparticles: size-dependent geometrical and electronic structure," J. Phys. Chem. C **116**, 7312–7317.

Revoy, M. N., Scott, R. W. J., and Grosvenor, A. P. (**2013**). "Ceria nanocubes: dependence of the electronic structure on synthetic and experimental conditions," J. Phys. Chem. C **117**, 10095–10105.

Shannon, R. D. (**1976**). "Revised effective ionic radii and systematic studies of interatomic distances in halides and chalcogenides," Acta Crystallogr. A **32**, 751–767.

Soykal, I. I., Sohn, H., and Ozkan, U. S. (**2012**). "Effect of support particle size in steam reforming of ethanol over Co/CeO_2 catalysts," ACS Catal. **2**, 2335–2348.

Sun, M., Zou, G., Xu, S., and Wang, X. (**2012**). "Nonaqueous synthesis, characterization and catalytic activity of ceria nanorods," Mater. Chem. Phys. **134**, 912–920.

Wang, Z. L. and Feng, X. (**2003**). "Polyhedral shapes of CeO_2 nanoparticles," J. Phys. Chem. B **107**, 13563–13566.

Wu, Z., Li, M., Howe, J., Meyer, H. M., and Overbury, S. H. (**2010**). "Probing defect sites on CeO_2 nanocrystals with well-defined surface planes by Raman spectroscopy and O_2 adsorption," Langmuir **26**, 16595–16606.

Wu, Z., Schwartz, V., Li, M., Rondinone, A. J., and Overbury, S. H. (**2012**). "Support shape effect in metal oxide catalysis: ceria-nanoshape-supported vanadia catalysts for oxidative dehydrogenation of isobutane," J. Phys. Chem. Lett. **3**, 1517–1522.

Zhou, K., Wang, X., Sun, X., Peng, Q., and Li, Y. (**2005**). "Enhanced catalytic activity of ceria nanorods from well-defined reactive crystal planes," J. Catal. **229**, 206–212.